

CONSTRAINING PHOSPHORUS CHEMISTRY IN CARBON- AND OXYGEN-RICH CIRCUMSTELLAR ENVELOPES: OBSERVATIONS OF PN, HCP, AND CP

S. N. MILAM,¹ D. T. HALFEN,² E. D. TENENBAUM,² A. J. APPONI,³ N. J. WOOLF,² AND L. M. ZIURYS²

Received 2007 August 7; accepted 2008 April 4

ABSTRACT

Millimeter-wave observations of PN, CP, and HCP have been carried out toward circumstellar envelopes of evolved stars using the Arizona Radio Observatory (ARO). HCP and PN have been identified in the carbon-rich source CRL 2688 via observations at 1 mm using the Submillimeter Telescope (SMT) and 2–3 mm with the Kitt Peak 12 m. An identical set of measurements were carried out toward IRC +10216, as well as observations of CP at 1 mm. PN was also observed toward VY Canis Majoris (VY CMa), an oxygen-rich supergiant star. The PN and HCP line profiles in CRL 2688 and IRC +10216 are roughly flat topped, indicating unresolved, optically thin emission; CP, in contrast, has a distinct “U” shape in IRC +10216. Modeling of the line profiles suggests abundances, relative to H₂, of $f(\text{PN}) \sim (3-5) \times 10^{-9}$ and $f(\text{HCP}) \sim 2 \times 10^{-7}$ in CRL 2688, about an order of magnitude higher than in IRC +10216. In VY CMa, $f(\text{PN})$ is $\sim 4 \times 10^{-8}$. The data in CRL 2688 and IRC +10216 are consistent with LTE formation of HCP and PN in the inner envelope, as predicted by theoretical calculations, with CP a photodissociation product at larger radii. The observed abundance of PN in VY CMa is a factor of 100 higher than LTE predictions. In IRC +10216, the chemistry of HCP/CP mimics that of HCN/CN and suggests an N₂ abundance of $f \sim 1 \times 10^{-7}$. The chemistry of phosphorus appears active in both carbon- and oxygen-rich envelopes of evolved stars.

Subject headings: astrobiology — astrochemistry — line: identification — stars: abundances — stars: chemically peculiar — stars: individual (CRL 2688; IRC +10216; VY CMa)

1. INTRODUCTION

Phosphorus plays a major role in biochemistry, being relevant to replication, metabolism, and structure in living systems (Pasek & Lauretta 2005). Yet it is not a particularly prevalent element, with a cosmic abundance relative to hydrogen of P/H $\sim 2.8 \times 10^{-7}$ (Grevesse & Sauval 1998), less than that of iron, magnesium, sodium, calcium, and aluminum. Despite this fact, phosphorus is a frequent constituent in iron meteorites, where its common form is an iron-nickel-phosphide compound called schreibersite ([Fe, Ni]₃P). Because of its concentrated presence in these types of meteorites, there is some thought that phosphorus needed for living systems was brought to Earth via meteoritic impact (Pasek & Lauretta 2005; Maciá 2005).

The history of phosphorus in interstellar gas is far less certain. This element is thought to be formed in massive stars ($M > 15 M_{\odot}$) during hydrostatic-shell C and Ne burning (Arnett 1996). It is released into the interstellar medium as these objects become supernovae. The rarity of high-mass stars has a direct effect on the low (solar) P abundance, as compared to other “biotic” elements such as C, N, and O (Maciá 2005), which are all formed in a larger stellar population. In diffuse clouds, gas-phase phosphorus has been found to have an abundance that is consistent with minimal depletion into a solid form, based on P II observations (Lebouteiller et al. 2005). In dense gas, on the other hand, large depletions have been claimed because the only phosphorus-bearing gas-phase molecule observed thus far has been PN (Ziurys 1987; Turner & Bally 1987; Turner et al. 1990). However,

it could be that phosphorus exists in other, as yet undiscovered, gaseous molecular forms.

In circumstellar envelopes, the state of phosphorus chemistry, until recently, has been similar to that in molecular clouds. CP was the only species observed, and it was only in one object, the carbon star IRC +10216 (Guélin et al. 1990). However, HCP has now been definitively detected in IRC +10216, and PN has been tentatively identified in this object as well, based on one clean and one blended transition (Agúndez et al. 2007). Furthermore, PN and PO have recently been observed in the shell of the oxygen-rich red supergiant, VY Canis Majoris (VY CMa; Ziurys et al. 2007; Tenenbaum et al. 2007). Thus, four phosphorus-bearing compounds have now been identified in circumstellar gas.

Here we present observations of phosphorus-bearing molecules in another circumstellar source, the carbon-rich post-asymptotic giant branch (AGB) star CRL 2688. PN and HCP have been conclusively detected in this object. An additional transition of PN has also been observed in IRC +10216, confirming the presence of this species toward this star, as well as several lines of HCP. (The HCP data were discovered independently of Agúndez et al. [2007], and were in preparation for submission when their detection was published.) Several transitions of PN in VY CMa and CP in IRC +10216 have been measured as well for comparison. In this paper we present our observations, derive molecular abundances, and discuss their implications for phosphorus chemistry in circumstellar envelopes.

2. OBSERVATIONS

The measurements were conducted during the period 2006 October through 2007 June at 1, 2, and 3 mm using the facilities of the Arizona Radio Observatory (ARO): the Kitt Peak 12 m and Submillimeter Telescope (SMT) at Mount Graham, Arizona. The 1 mm observations were carried out at the SMT with a dual-polarization ALMA Band 6 receiver system employing sideband-separating mixers with an image rejection of typically 15–20 dB. The back end was a 2048 channel 1 MHz filter bank, used in

¹ SETI Institute, NASA Ames Research Center, MS 245-6, Moffett Field, CA 94035-1000; stefanie.n.milam@nasa.gov.

² Department of Chemistry, Department of Astronomy, NASA Astrobiology Institute, Steward Observatory, The University of Arizona, 933 North Cherry Avenue, Tucson, AZ 85721; halfendt@as.arizona.edu, emilyt@as.arizona.edu, nwoolf@as.arizona.edu, lziurys@as.arizona.edu.

³ GEOST 7526 North Cholla Boulevard, Tucson, AZ 85741; aapponi@gmail.com.

TABLE 1
OBSERVATIONS OF PHOSPHORUS SPECIES TOWARD CIRCUMSTELLAR ENVELOPES

Source	Molecule	Transition	Frequency (MHz)	η_b or η_c^a	θ_b (arcsec)	T_R (K)	$\Delta V_{1/2}$ (km s $^{-1}$)	V_{LSR} (km s $^{-1}$)	$\int T_R dV$ (K km s $^{-1}$)
CRL 2688 ^b	PN	$J = 2 \rightarrow 1$	93979.8	0.88	67	0.003 ± 0.002	25.5 ± 6.4	-36.8 ± 6.2	0.061
		$J = 3 \rightarrow 2^c$	140967.8	0.76	44	~ 0.007	~ 36	~ -38	0.118
	HCP	$J = 5 \rightarrow 4$	234935.7	0.78	32	0.009 ± 0.005	32.0 ± 2.6	-37.4 ± 2.6	0.253
		$J = 4 \rightarrow 3$	159802.6	0.72	39	0.012 ± 0.006	29.5 ± 3.8	-34.0 ± 3.8	0.354
		$J = 6 \rightarrow 5$	239693.8	0.78	31	0.019 ± 0.009	35.0 ± 2.5	-35.9 ± 2.5	0.463
		$J = 7 \rightarrow 6$	279634.7	0.78	27	0.028 ± 0.010	28.9 ± 3.2	-34.4 ± 3.2	0.758
		$J = 2 \rightarrow 1$	93979.8	0.88	67	0.007 ± 0.001	28.7 ± 6.4	-27.5 ± 6.4	0.177
IRC +10216 ^d	PN	$J = 3 \rightarrow 2^c$	140967.8	0.76	44	~ 0.011	~ 34	~ -24	0.221
		$J = 5 \rightarrow 4$	234935.7	0.78	32	0.010 ± 0.003	29.4 ± 2.6	-27.3 ± 2.6	0.229
	HCP	$J = 4 \rightarrow 3$	159802.6	0.72	39	0.010 ± 0.003	24.5 ± 3.8	-26.9 ± 3.8	0.233
		$J = 5 \rightarrow 4$	199749.4	0.78	38	0.010 ± 0.005	~ 27	~ -27	0.241
		$J = 6 \rightarrow 5$	239693.8	0.78	31	0.021 ± 0.005	27.5 ± 2.2	-26.6 ± 2.2	0.549
		$J = 7 \rightarrow 6$	279634.7	0.78	27	0.028 ± 0.008	27.9 ± 2.1	-27.1 ± 2.1	0.760
		$N = 5 \rightarrow 4$
	CP	$J = 5.5 \rightarrow 4.5^c$	238856.5	0.78	32	~ 0.012	~ 38	~ -27	0.500
		$J = 4.5 \rightarrow 3.5$	238303.1	0.78	32	0.006 ± 0.002	27.6 ± 5.0	-27.2 ± 2.5	0.197
		$J = 6 \rightarrow 5$	281914.1	0.78	27	0.017 ± 0.006	34.1 ± 4.2	18.6 ± 4.2	0.487
VY CMa ^e	PN	$J = 3 \rightarrow 2$	140967.8	0.76	44	0.003 ± 0.001	~ 40	18.5 ± 8.5	0.120
		$J = 5 \rightarrow 4$	234935.7	0.78	32	0.012 ± 0.004	37.1 ± 5.1	16.7 ± 5.1	0.473
		$J = 6 \rightarrow 5$	281914.1	0.78	27	0.017 ± 0.006	34.1 ± 4.2	18.6 ± 4.2	0.487

NOTE.—All data measured with the SMT except the $J = 2 \rightarrow 1, 3 \rightarrow 2$ lines of PN and the $J = 4 \rightarrow 3$ line of HCP, which were observed with the ARO 12 m telescope.

^a η_b and for SMT measurements and η_c and for 12 m data.

^b $\alpha = 21^{\text{h}}00^{\text{m}}20.0^{\text{s}}$, $\delta = 36^{\circ}29'44''$ (B1950.0).

^c Blended feature (see text).

^d $\alpha = 09^{\text{h}}45^{\text{m}}14.8^{\text{s}}$, $\delta = 13^{\circ}30'40''$ (B1950.0).

^e $\alpha = 07^{\text{h}}20^{\text{m}}54.7^{\text{s}}$, $\delta = -25^{\circ}40'12''$ (B1950.0).

parallel (2×1024) mode. The temperature scale at the SMT is T_A^* ; radiation temperature is then defined as $T_R = T_A^*/\eta_b$, where η_b is the main-beam efficiency. The 2 and 3 mm observations were conducted at the ARO 12 m using dual-polarization SIS mixers, operated in single-sideband mode with the image rejection ≥ 20 dB. Filter banks with 512 channels of 1 and 2 MHz resolutions were used simultaneously in parallel mode for the measurements, along with an autocorrelator with 782 kHz resolution. The intensity scale of the 12 m is the chopper-wheel corrected antenna temperature, T_R^* , including forward spillover losses, which is converted to radiation temperature by $T_R = T_R^*/\eta_c$, where η_c is the corrected beam efficiency. Data were taken in beam-switching mode with a subreflector throw of $\pm 2'$. Pointing and focus was monitored regularly by observations of nearby planets and quasars. Source coordinates, rest frequencies, telescope efficiencies, and beam sizes are given in Table 1.

3. RESULTS

The data obtained for CRL 2688 are presented in Figure 1. As shown, three rotational transitions were detected individually for HCP and PN toward this object. The $J = 2 \rightarrow 1$ and $3 \rightarrow 2$ lines of PN and the $J = 4 \rightarrow 3$ transition of HCP were measured at the ARO 12 m, while the $J = 6 \rightarrow 5$ and $7 \rightarrow 6$ lines of HCP, as well as the $J = 5 \rightarrow 4$ transition of PN, were observed at the SMT. As shown in Table 1, all features have local standard of rest (LSR) velocities in the range -34 to -37 km s $^{-1}$, and line widths of ~ 35 km s $^{-1}$, typical parameters for CRL 2688 (e.g., Sopka et al. 1989; Young et al. 1992). The intensities are also consistent among the transitions. The HCP line profiles are roughly flat topped with evidence of a slight U shape, with stronger emission on the blueshifted side. This profile indicates unresolved, or partially resolved, optically thin emission. Observations of other molecules in CRL 2688 suggest a roughly spherical, AGB “remnant” flow of $\sim 20''$ – $30''$ (Nguyen-Q-Rieu et al. 1984; Fukasaku et al.

1994; Highberger et al. 2003). The three transitions of HCP were measured with a beam size of $\leq 39''$, consistent with the extent of the remnant wind. Slight asymmetries are also present in line profiles from species arising in this flow, such as NaCl, NH₃, and HC₇N. Some of these asymmetries may result from the additional outflows present in CRL 2688, caused by an erratic, second phase of mass loss, which distorts the remnant AGB wind (e.g., Cox et al. 1997, 2000). The PN profiles are also flat topped in shape, although there is again evidence of a U in the $J = 5 \rightarrow 4$ line, observed with the smallest beam of $32''$. The $J = 3 \rightarrow 2$ transition of PN is unfortunately blended with ³⁰SiC₂ at 140956.2 MHz, with the $J_{K_a, K_c} = 9_{3,6} \rightarrow 8_{3,5}$ transition of NaCN nearby at 140937.8 MHz.

In Figure 2, the same transitions of PN and HCP are shown for IRC +10216. The $J = 3 \rightarrow 2$ transition of PN is contaminated by ³⁰SiC₂, as in CRL 2688, but the $J = 5 \rightarrow 4$ line is clean and confirms the presence of this species in IRC +10216. The LSR velocities and line widths found for these molecules are characteristic of this object (see Table 1; Cernicharo et al. 2000). The data from this source display the classic, flat-topped profile, suggesting that the emission is unresolved and optically thin. Agúndez et al. (2007) found slight U shapes in corresponding HCP spectra obtained with the IRAM 30 m telescope. These authors derived a source of roughly $12''$ – $30''$, consistent with the ARO beam sizes at these frequencies for unresolved emission.

Figure 3 displays the $J = 3 \rightarrow 2, 5 \rightarrow 4$, and $6 \rightarrow 5$ transitions of PN toward VY CMa. All three lines of this molecule appear to exhibit somewhat triangular line profiles, likely coming from an ellipsoidal wind that is elongated in the plane of the sky (see Ziurys et al. 2007). PN is the first phosphorus-bearing species identified in an oxygen-rich, as opposed to carbon-rich, envelope. The initial detection of phosphorus nitride in this source was mentioned briefly in Ziurys et al. (2007), where the $J = 5 \rightarrow 4$ spectra was presented.

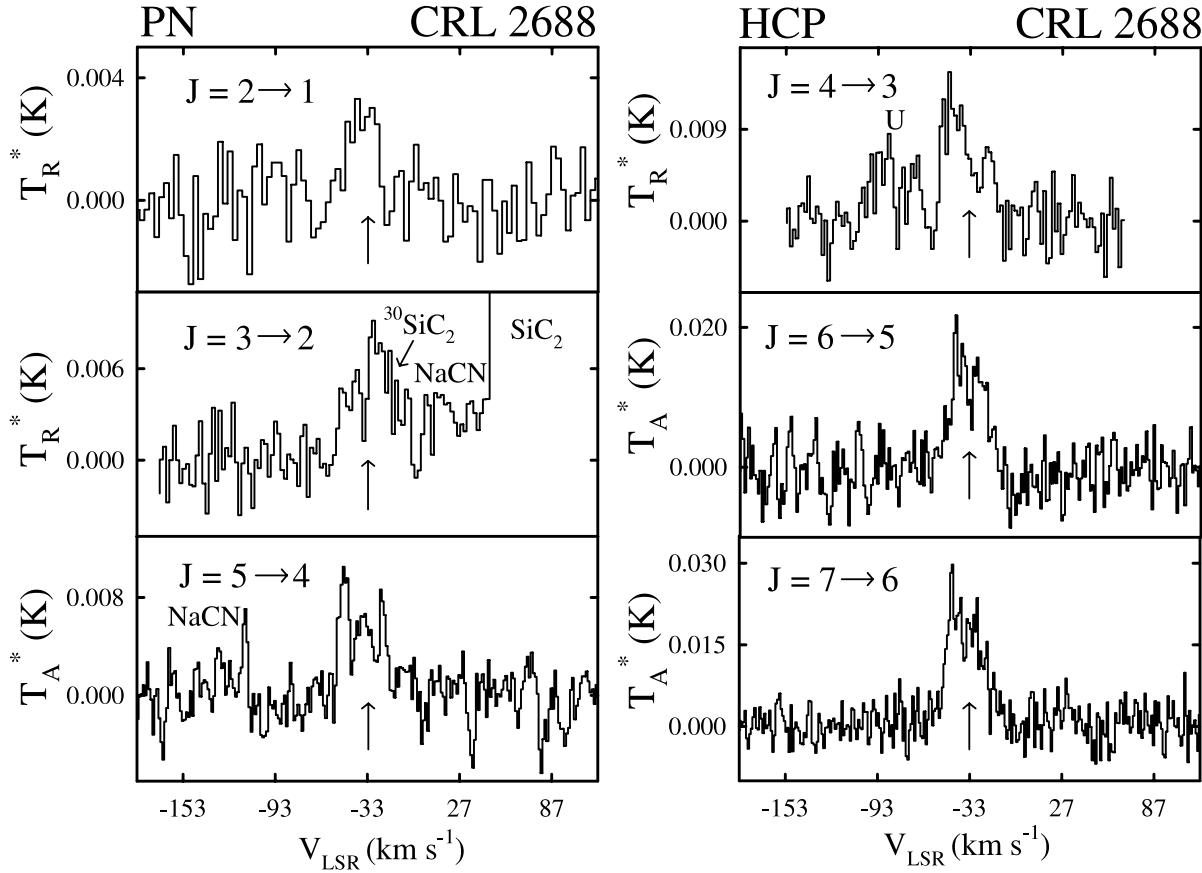


FIG. 1.—Spectra obtained for PN and HCP toward CRL 2688, using the ARO 12 m and SMT telescopes. Right: $J = 4 \rightarrow 3$, $6 \rightarrow 5$, and $7 \rightarrow 6$ transitions of HCP at 160, 240, and 280 GHz, which all display a slightly asymmetric U shape. Left: $J = 2 \rightarrow 1$, $3 \rightarrow 2$, and $5 \rightarrow 4$ transitions of PN at 94, 141, and 235 GHz. The $J = 3 \rightarrow 2$ line of PN is contaminated by $^{30}\text{SiC}_2$, but the other two transitions are fairly flat topped, considering the signal-to-noise ratios. The PN $J = 2 \rightarrow 1$ and $J = 3 \rightarrow 2$, as well as the HCP $J = 4 \rightarrow 3$ lines, were obtained with the 12 m telescope, while the other spectra were measured at the SMT. All spectra were obtained with 1 MHz resolution. These measurements are clear evidence that these two phosphorus-bearing compounds are present toward CRL 2688.

For comparison, observations of the $N = 5 \rightarrow 4$ lines of CP were also carried out toward IRC +10216; see Figure 4. This radical was originally detected in this source by Guélin et al. (1990), who measured several transitions. In Figure 4, the two fine-structure components of the $N = 5 \rightarrow 4$ transition are shown. Each component consists of two hyperfine lines, but these are separated at most by 1.5 channels in the resolution displayed, and therefore do not affect the line shape. While the $J = 5.5 \rightarrow 4.5$ feature is blended with the spin-rotation doublets of $^{13}\text{CCCCH}$ (*top panel*), the $J = 4.5 \rightarrow 3.5$ component is uncontaminated (*bottom panel*), and appears to be somewhat U shaped. Guélin et al. (1990) had suggested that this line was flat topped, but the signal-to-noise ratio is better in the current data shown here. Additional observations would help clarify this issue. If real, the U shape would again indicate a resolved, optically thin distribution and hence a source size of $\sim 32''$.

A complete summary of line parameters for all spectra is given in Table 1. These values include the measured main-beam brightness temperature, the FWHM line width, the LSR velocity, and the integrated intensity.

4. ANALYSIS

4.1. Circumstellar Radiative Transfer Code

In order to establish molecular abundances and spatial distributions, the radiative transfer code of Bieging & Tafalla (1993) was used. In this model, a set of statistical equilibrium equations are solved for populating rotational levels of a given molecule

assuming a spherically expanding circumstellar shell. Input parameters necessary for the modeling are distance to the object, outflow velocity, mass-loss rate, and temperature and density profiles. The gas temperature profile was modeled

$$T_{\text{kin}} = T_{\text{kin}0} \left(\frac{r}{r_{\text{kin}0}} \right)^{-0.7}. \quad (1)$$

The initial temperature, $T_{\text{kin}0}$, was assumed to be the effective temperature of the star and $r_{\text{kin}0}$ was defined as the stellar radius. The exponent value of -0.7 was chosen on the basis of other profiles from evolved stars (see Kemper et al. 2003; Keady et al. 1988). A density distribution dependence of r^{-2} was used for all model calculations, and the outflow velocity was established individually from the line profiles for a given species. Collisional cross sections for PN have been recently calculated by Tobola et al. (2007) and were incorporated into the model. Cross sections for HCP or CP are not known; thus, values for HCN and PN were used, respectively.

The model was used to reproduce the observed line profiles by varying two parameters: the molecular abundance relative to H_2 and the radial source distribution. Both Gaussian and shell distributions were considered. For the Gaussian model, the expression describing the abundance distribution is given by

$$f(r) = f(X) e^{-(r/r_{\text{refold}})^2}, \quad (2)$$

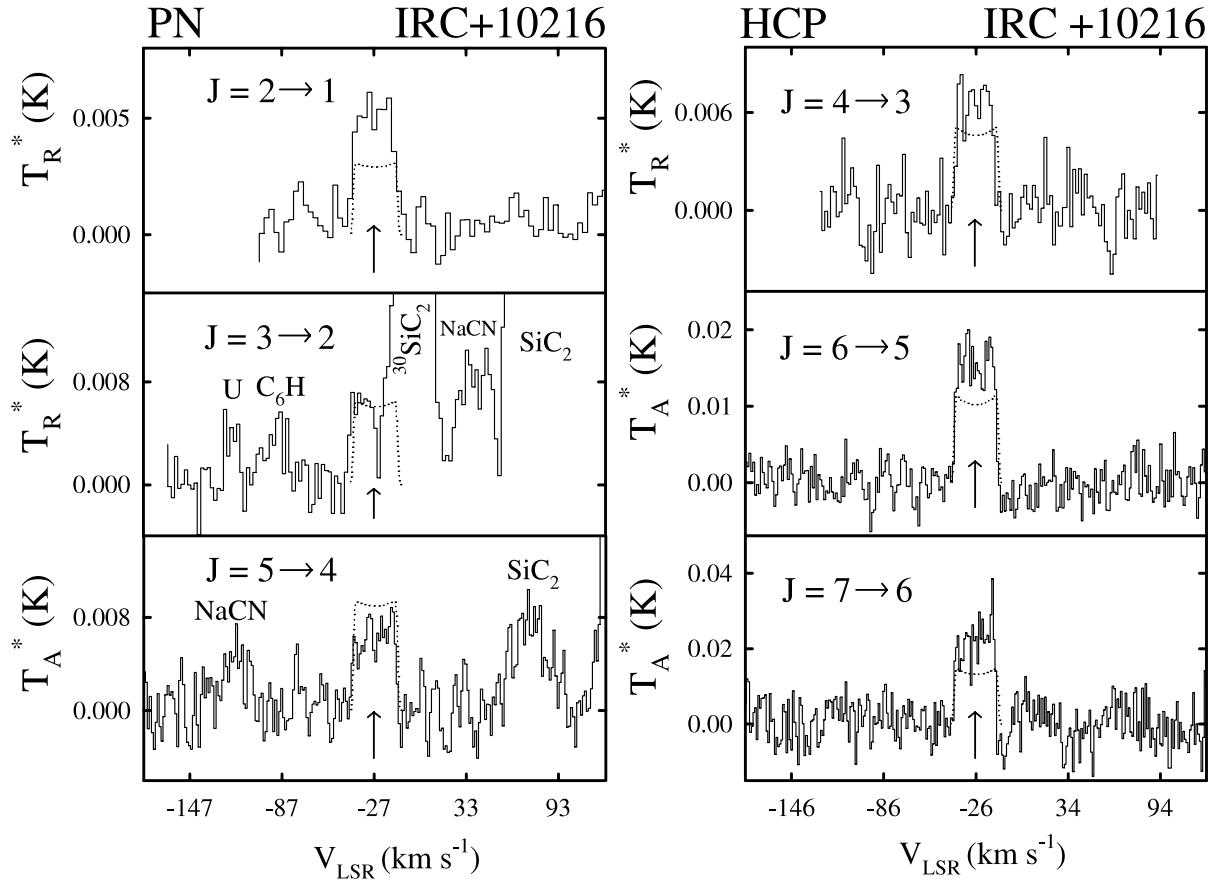


FIG. 2.—Set of spectra identical to that in Fig. 1, but observed toward IRC+10216. In this source, all lines display a flat-topped profile indicating optically thin, unresolved emission. The $J = 3 \rightarrow 2$ line of PN (*left*) appears as a shoulder on the $^{30}\text{SiC}_2$ feature. All data were taken with 1 MHz resolution. The model fits are shown by the dashed lines on the spectra.

where $f(X)$ is the central abundance of a specific molecule and r_{efold} is the radius where the abundance decreases by $1/e$. For the shell distribution, the abundance function is

$$f(r) = f(X)e^{-[(r-r_{\text{max}0})/r_{\text{efold}}]^2}. \quad (3)$$

In this case, $f(X)$ is the maximum abundance of the specified species, $r_{\text{max}0}$ is the corresponding radius, and r_{efold} is the distance from $r_{\text{max}0}$ where the abundance decreases by $1/e$. Three rotational transitions per molecule were simultaneously fit in most cases in order to constrain the model variables, except in the case of severe line contamination. When available, additional spectra from the literature were incorporated into the modeling.

The model fit for each source was determined by visual inspection. For the individual molecules in each envelope, the source distribution was successively varied in increments of $5''$ and the abundance adjusted to obtain the best match to the observed spectrum.

The dipole moments used for PN, HCP, and CP were 2.75, 0.39, and 0.86 D, respectively (Pickett et al. 1998; Müller et al. 2005; Rohlfs & Almlöf 1988). Einstein A -coefficients were derived using these values and the appropriate dipole matrix element. Energy levels were calculated from the individual molecular rotational constants, which are listed in the JPL catalog (Pickett et al. 1998).

4.2. Modeling of Observed Sources

Because independent estimates of source sizes were available for IRC+10216, these data were modeled first. The fitting

parameters assumed for IRC+10216 were a mass-loss rate of $3 \times 10^{-5} M_\odot \text{ yr}^{-1}$, an effective stellar temperature of $T_{\text{eff}} \sim 2320 \text{ K}$, a stellar radius of $R_* \sim 6.5 \times 10^{13} \text{ cm}$, and a distance of 150 pc (Agúndez & Cernicharo 2006). A fit to eight observed profiles of HCP (1 transition ARO 12 m; 3 transitions SMT; 4 transitions IRAM) yielded an e -folding radius of $2.5 \times 10^{16} \text{ cm}$ ($\theta_s = 22''$), assuming a spherical geometry, and a fractional abundance relative to H_2 of $f \sim 3 \times 10^{-8}$. For PN, three spectral profiles were fit ($J = 2 \rightarrow 1$, Guélin et al. [2000] and ARO 12 m; $J = 5 \rightarrow 4$, SMT), yielding a source radius of $4 \times 10^{16} \text{ cm}$ ($\theta_s \sim 36''$) for a spherical distribution and a fractional abundance of $f \sim 3 \times 10^{-10}$. Shell geometries were also attempted in the analysis of the HCP and PN profiles, but were not as successful in reproducing these spectra. In the case of CP, only one transition could be reliably modeled: the $J = 4.5 \rightarrow 3.5$ component of the $N = 5 \rightarrow 4$ line. The other lines of CP observed in this work or by Guélin et al. (1990) were contaminated. In this case, both the IRAM and SMT data were modeled with a shell distribution. The shell source is consistent with the predictions of Agúndez et al. (2007) and the U shape observed at the SMT. The best fit to the two data sets suggests that CP arises from a shell approximately $4 \times 10^{16} \text{ cm}$ wide ($18''$ wide), with a peak abundance of $f \sim 1 \times 10^{-8}$ at a radius of $\sim 3 \times 10^{16} \text{ cm}$ ($r \sim 13''$). The modeled spectra for all three molecules are overlaid on the observed lines in Figures 2 and 3.

For CRL 2688, the model parameters employed in the analysis are a distance of 1000 pc, $R_* \sim 9 \times 10^{12} \text{ cm}$, $T_{\text{eff}} \sim 6500 \text{ K}$, and a mass-loss rate of $1.7 \times 10^{-4} M_\odot \text{ yr}^{-1}$ (Skinner et al. 1997; Truong-Bach et al. 1990). The spectra for both PN and HCP were

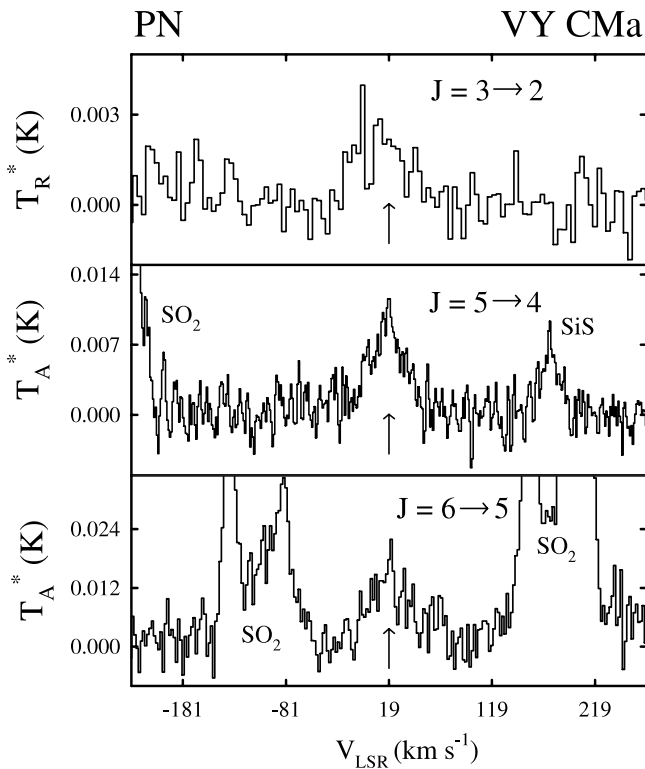


FIG. 3.—Spectra of PN observed toward VY CMa. The $J = 5 \rightarrow 4$ and $6 \rightarrow 5$ transitions were measured with the SMT at 235 and 282 GHz, respectively, with a resolution of 1 MHz. The $J = 3 \rightarrow 2$ line at 141 GHz was obtained at the ARO 12 m telescope and observed with 2 MHz resolution. The line profiles are triangular, tracing a roughly ellipsoidal wind in VY CMa. (The $J = 5 \rightarrow 4$ spectrum was previously published in Ziurys et al. [2007].)

constrained as flat-topped profiles with a spherical distribution. The best fit to the data for HCP yielded an abundance of $f \sim 2 \times 10^{-7}$ and $r_{\text{efold}} \sim (6-9) \times 10^{16} \text{ cm}$ ($\theta_s \sim 8''-12''$) and $f \sim (3-5) \times 10^{-9}$ with $r_{\text{efold}} \sim (6-15) \times 10^{16} \text{ cm}$ ($\theta_s \sim 8''-20''$) for PN.

In the case of VY CMa, the distance was set at 1500 pc, with a mass-loss rate of $\sim 10^{-4} M_\odot \text{ yr}^{-1}$, $T_{\text{eff}} \sim 3368 \text{ K}$, and a stellar radius of $R_* \sim 1.36 \times 10^{14} \text{ cm}$ (Humphreys et al. 2007). The total mass-loss rate in this object is $(2-4) \times 10^{-4} M_\odot \text{ yr}^{-1}$ (Monnier et al. 1999), but PN only appears in one of the three flows that contribute to the loss of material (see Ziurys et al. 2007). A fit to three transitions of PN resulted in $f \sim 4 \times 10^{-8}$ for a source radius of $r_{\text{efold}} \sim 1 \times 10^{16} \text{ cm}$ ($\theta_s \sim 1''$).

The derived source sizes, fractional abundances, and corresponding column densities are listed in Table 2.

4.3. Quality of the Model

In Table 3, the observed and predicted line integrals are given in order to evaluate the model fits. The difference between the observed and modeled values is typically 10%–30%. The excitation analysis from the model suggests that most of the observed transitions are subthermal in the outer envelope. For CP and HCP, the initial excitation temperatures closely follow the gas kinetic temperature ($T_{\text{ex}} \cong T_{\text{kin}}$), but become subthermal ($T_{\text{ex}} < T_{\text{kin}}$) at larger radii as the density decreases. In the case of PN, T_{ex} followed the kinetic temperature in the inner part of the shells, became slightly superthermal ($T_{\text{ex}} > T_{\text{kin}}$) midway through the envelopes, and then reverted to subthermal in the outer part. There are no opacity effects in any of the molecules, because all emission is optically thin.

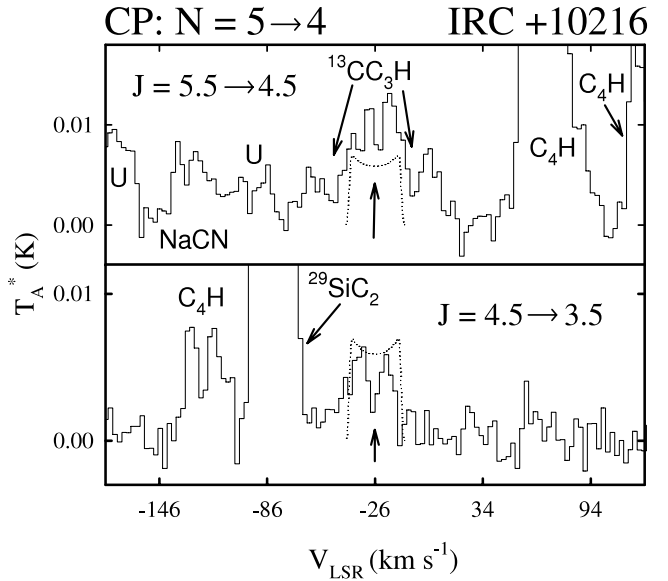


FIG. 4.—Spectra of the $J = 5.5 \rightarrow 4.5$ (top) and the $J = 4.5 \rightarrow 3.5$ (bottom) fine-structure components of the $N = 5 \rightarrow 4$ transition of CP observed with the SMT at 238 GHz toward IRC+10216. Each component consists of two hyperfine lines which are split by no more than 3 MHz, and hence do not impact the line profiles. The $J = 5.5 \rightarrow 4.5$ line is severely contaminated by the two fine structure components of $^{13}\text{CCCCH}$, as indicated by the arrows. The $J = 4.5 \rightarrow 3.5$ line profile appears U shaped, indicating thin, resolved emission. These data were measured with 1 MHz filters and smoothed to a 2 MHz resolution. Model results are shown by the dashed lines on the spectra.

The fractional abundances and source sizes are fairly well constrained. A $5''$ change in the source size resulted in a noticeable degradation of the fit. Changes in abundances of 50% also produced poorer fits. The analysis was also not particularly sensitive to the temperature profile used. For example, using a different profile found in Bieging et al. (2000), which increases the kinetic temperature at a given radius by about an order of magnitude, resulted in only a factor of 2 change in abundance. Such tests suggest that the fractional abundances are probably constrained to within a factor of 3 and the source sizes to within $5''$.

The influence of the infrared field from the star and the dust emission was considered but not used in the final analysis. Unlike HCN, integrated infrared absorption intensities, which are related to the dipole moment derivative matrix elements, are not well known for these molecules. Hence, the Einstein A -coefficients for vibrational decay are uncertain. To evaluate the possible effect of IR radiation, the $v_2 = 1$ state of HCP was considered in the model calculations. This vibrational state lies the lowest in energy of all vibrational levels of HCP, PN, and CP (Beck et al. 2000; Ahmad & Hamilton 1995; Ram et al. 1992), and it is most likely to be excited. The dipole moment derivative for the v_2 mode of HCP was scaled from that of HCN. Using this estimated dipole moment derivative, and the infrared field of Bieging & Tafalla (1993), a 5%–10% decrease in the HCP abundance results in the modeling. This difference is well within the uncertainties that occur from the use of scaled matrix elements. Infrared excitation does not appear to be a dominating factor influencing the abundances for these molecules, although there are many unknown factors.

5. DISCUSSION

5.1. Active Phosphorus Chemistry in Circumstellar Envelopes

The detection of HCP and PN in another circumstellar envelope, CRL 2688, coupled with the results in IRC+10216 (CP,

TABLE 2
COLUMN DENSITIES AND ABUNDANCES OF CIRCUMSTELLAR PHOSPHORUS-BEARING MOLECULES

Source	Molecule	θ_s (arcsec)	e-folding Radius (cm)	N_{tot} (cm $^{-2}$)	$f(X/H_2)$
VY CMa	PN	1	1×10^{16}	2×10^{15}	4×10^{-8}
	PO ^a	1	1×10^{16}	3×10^{15}	9×10^{-8}
CRL 2688	PN	8–20	$(0.6–1.5) \times 10^{17}$	$(5–8) \times 10^{15}$	$(5–3) \times 10^{-9}$
	HCP	8–12	$(6–9) \times 10^{16}$	3×10^{17}	2×10^{-7}
IRC +10216	PN	36	4×10^{16}	1×10^{13}	3×10^{-10}
	HCP	22	2×10^{16}	1×10^{15}	3×10^{-8}
	CP	26 (shell) ^b	$(1–5) \times 10^{16}$ (shell) ^b	1×10^{14}	1×10^{-8}

^a Abundance and source size from Tenenbaum et al. (2007).

^b Shell distribution described by eq. (3) where $r_{\text{max}0} = 3 \times 10^{16}$ cm and $r_{\text{efold}} = 2 \times 10^{16}$ cm.

PN, HCP; Guélin et al. 1990; Agúndez et al. 2007) and VY CMa (PN, PO; Ziurys et al. 2007; Tenenbaum et al. 2007), suggest that gas-phase phosphorus chemistry in these types of objects may be relatively complex. Phosphorus as an element is not particularly abundant, as mentioned, and it is thought to be refractory, as suggested by condensation models (Lodders & Fegley 1999). Moreover, this element is formed primarily in neon burning of massive stars, where it is released during Type II supernovae (Clayton 2003). Therefore, there should be little overproduction of phosphorus in IRC +10216 or CRL 2688. Because VY CMa is quite massive and is thought to be on the track to becoming a supernova (Richards et al. 1998), there may be some enhancement of this element in this object, depending on the degree of dredge-up. Measurements of the $^{12}\text{C}/^{13}\text{C}$ ratio toward this source imply ratios in the range of 25–46 (Milam et al. 2008), suggesting that considerable mixing from the stellar interior may have occurred. How this process affects the phosphorus abundance is unknown.

Assuming solar abundance ($\text{P/H} \sim 3 \times 10^{-7}$), and neglecting the possible presence of other phosphorus-bearing species, about 7% of the available phosphorus is in the form of gas-phase molecules toward IRC +10216, and about 33% in CRL 2688. In VY CMa, the percentage is $\sim 21\%$. The higher amounts of gas-

phase phosphorus in CRL 2688 and VY CMa may result from the energetic outflows present in both of these sources (Humphreys et al. 2007; Skinner et al. 1997), which could be destroying phosphorus-bearing grains. Both PN and PO, however, appear to arise from the more quiescent wind in VY CMa, as opposed to the red- and blueshifted flows that apparently correlate with sporadic mass-loss events (see Ziurys et al. 2007). In CRL 2688, the suggestion of asymmetries in the profiles of HCP and PN may link these species in part to some of the fast winds in this object, but higher sensitivity spectra and/or maps are needed to examine this possibility more thoroughly. Alternatively, IRC +10216 may contain additional but unknown molecular forms of phosphorus. Further observations may yield additional species that raise the gas-phase component of this element.

5.2. Theoretical Predictions of Phosphorus-bearing Molecules

The current models of circumstellar phosphorus chemistry available in the literature use the same approach: certain species are formed at LTE near the stellar photosphere, as “parent molecules”; as these compounds flow into the outer envelope, photochemistry creates radicals and ions. In the oxygen-rich model of Willacy & Millar (1997), LTE chemistry produces a single important parent molecule, PH_3 , which then reacts to

TABLE 3
OBSERVED AND PREDICTED INTEGRATED LINE INTENSITIES

Source	Molecule	Transition	Observed $\int T_R dV$ (K km s $^{-1}$)	Predicted $\int T_R dV$ (K km s $^{-1}$)
CRL 2688	PN	$J = 2 \rightarrow 1$	0.061 ± 0.012	$0.090–0.110$
		$J = 3 \rightarrow 2^a$	0.118 ± 0.019	$0.176–0.245$
		$J = 5 \rightarrow 4$	0.253 ± 0.013	$0.196–0.305$
	HCP	$J = 4 \rightarrow 3$	0.354 ± 0.023	$0.406–0.542$
		$J = 6 \rightarrow 5$	0.463 ± 0.022	$0.524–0.593$
		$J = 7 \rightarrow 6$	0.758 ± 0.032	$0.566–0.612$
IRC +10216	PN	$J = 2 \rightarrow 1$	0.177 ± 0.006	0.098
		$J = 3 \rightarrow 2^a$	0.221 ± 0.034	0.238
		$J = 5 \rightarrow 4$	0.229 ± 0.008	0.340
	HCP	$J = 4 \rightarrow 3$	0.233 ± 0.011	0.194
		$J = 5 \rightarrow 4$	0.241 ± 0.020	0.252
		$J = 6 \rightarrow 5$	0.549 ± 0.011	0.398
		$J = 7 \rightarrow 6$	0.760 ± 0.017	0.514
	CP	$N = 5 \rightarrow 4$
		$J = 5.5 \rightarrow 4.5^a$	0.500 ± 0.015	0.258
		$J = 4.5 \rightarrow 3.5$	0.197 ± 0.010	0.212
VY CMa	PN	$J = 3 \rightarrow 2$	0.120 ± 0.020	0.101
		$J = 5 \rightarrow 4$	0.473 ± 0.020	0.361
		$J = 6 \rightarrow 5$	0.487 ± 0.025	0.508

^a Blended feature (see text).

create PH, PH₂, P, P⁺, and finally PO at radii of $r \sim 10^{16}$ – 10^{17} cm. PH₃ and P⁺ remain the most abundant species, with $f \sim 3 \times 10^{-8}$, relative to H₂. The peak abundance for PO is $f \sim 3 \times 10^{-10}$. The computations of MacKay & Charnley (2001) consider both the carbon- and oxygen-rich cases. For the C-rich envelope, these authors predict HCP as the exclusive parent species, which photodissociates to create CP, P, and P⁺ again at radii of 10^{16} – 10^{17} cm. In the O-rich scheme, the only major parent molecule is PS, which leads to the photodissociation products P, P⁺, and PO at similar radii. The maximum abundance of PO is $f \sim 10^{-9}$ at $r \sim 2 \times 10^{16}$ cm.

A more recent model by Agúndez et al. (2007) predicts a somewhat different set of abundances. In the O-rich case, PO is the most prevalent species at ~ 2 stellar radii (R_*) with $f \sim 10^{-7}$, and PS attaining an equivalent abundance at $\sim 3 R_*$. Beyond a radius of $\sim 4 R_*$, P₄O₆ becomes the only significant phosphorus carrier. The abundance of PN never exceeds $f \sim 10^{-10}$. In the carbon-rich scenario, the Agúndez et al. (2007) model predicts HCP to be the major phosphorus-bearing species at $r \leq 10 R_*$, with $f \sim 10^{-7}$. Following the chemistry through the envelope, HCP gradually reacts to form CP, HC₃P, and PN at radii of 10^{16} – 10^{17} cm, with $f(\text{CP}) \sim 3 \times 10^{-9}$ and $f(\text{PN}) \sim 2 \times 10^{-9}$. The abundance of HCP then drops to $f \sim 10^{-8}$. All molecules are photodissociated at $r \sim 10^{17}$ cm.

For comparison, LTE abundance calculations for P-containing species were carried out in this work, using an expanded model of Tsuji (1973), described in Turner et al. (1990). The model is the original (Tsuji 1973) version but updated to include phosphorus chemistry. The computations were done for O-rich (solar: C/O ~ 0.5) and C-rich (C/O ~ 1.5) abundances, over the range of temperatures from 600 to 3000 K with a particle density of $n \sim 10^{11} \text{ cm}^{-3}$. The results of these calculations are presented in Figure 5. The condensation temperature of schreibersite ([Fe, Ni]₃P), the main solid state carrier of phosphorus, is ~ 1800 K at these pressures (Lodders & Fegley 1999). At this temperature, carbon-rich LTE chemistry predicts $f(\text{HCP}) \sim 10^{-8}$, with $f(\text{CP}) \sim f(\text{PN}) \sim 3 \times 10^{-10}$. In the O-rich model, PO is the main phosphorus species with $f \sim 5 \times 10^{-8}$, followed by PN and PS, both with $f \sim 5 \times 10^{-10}$.

5.3. Comparison with Observations

In IRC +10216, the behaviors of both HCP and CP are well predicted by the model of Agúndez et al. (2007). The observed abundance of HCP is $f \sim 3 \times 10^{-8}$, with $r \sim 11''$ or 2.5×10^{16} cm ($\sim 380 R_*$), while $f(\text{CP}) \sim 1 \times 10^{-8}$ and has a shell distribution with $r \sim 13''$ (3×10^{16} cm). On the other hand, PN has $f \sim 3 \times 10^{-10}$, about an order of magnitude less than the Agúndez et al. (2007) prediction. However, this abundance matches the LTE value calculated here at 1800 K (see Fig. 5). This result suggests that PN is not produced by nonequilibrium photochemistry in the outer envelope of IRC +10216, but instead is created close to the star under LTE conditions. The abundance then “freezes out” until the molecule is photodissociated. The PN line profiles are consistent with a spherical distribution, supporting the freezeout scenario.

In CRL 2688, the abundances of PN and HCP are both about 1 order of magnitude higher than in IRC +10216, but the PN/HCP ratio is roughly the same (~ 0.01 – 0.02). Both HCP and PN have extended distributions with radii of $\sim (1\text{--}2) \times 10^{17}$ cm [$(1\text{--}2) \times 10^4 R_*$], consistent with an older, larger shell. To a first approximation, the chemistry of these two species mimics that of IRC+10216, with LTE formation, but at a lower condensation temperature of ~ 1600 K instead of 1800 K (see Fig. 5). The shock activity in this post-AGB envelope may be keeping material

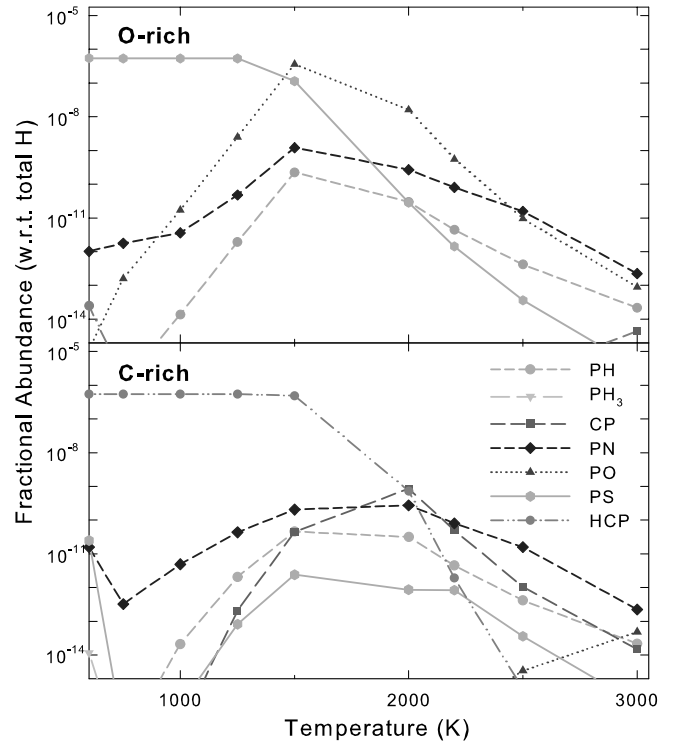


FIG. 5.—LTE abundances relative to the total hydrogen (H₂ + H + H⁺) as a function of temperature for the phosphorus chemical network, predicted using a modified version of the model by Tsuji (1973). Calculations were made for the O-rich (C/O ~ 0.5 ; top) and C-rich (C/O ~ 1.5 ; bottom) cases at a density of $n \sim 10^{11} \text{ cm}^{-3}$. At the phosphorus condensation temperature of 1800 K, HCP is the dominant species in the carbon-rich model, while PO is for the oxygen-rich prediction.

from condensing onto grains longer than in IRC +10216, lowering the effective condensation temperature. However, the PN abundance from the model at the lower temperature is still about an order of magnitude too low. Perhaps a more active photochemistry is also contributing to the formation of PN in CRL 2688, caused by the more advanced stage of mass loss, which has exposed a hotter star.

In VY CMa, PN and PO have abundances of 4×10^{-8} and 9×10^{-8} in a $1''$ region. At the distance of this object, this distribution corresponds to a radius of $r \sim 10^{16}$ cm, or $\sim 75 R_*$. The abundance of PO in VY CMa is very well predicted by the LTE model at 1800 K (see Fig. 5). However, the prediction of PN is about 2 orders of magnitude too low. Even at its maximum calculated value at 1000 K, the abundance of PN only reaches $\leq 10^{-9}$, about a factor of 15 less than that observed.

Given the assumed solar abundance of 3×10^{-7} , not all the phosphorus in VY CMa is confined to PO. According to the LTE calculations, PS is the next important sink for this element. However, this radical has yet to be observed in VY CMa. SiS is quite abundant in the spherical wind of this object, with $f \sim 10^{-6}$ (Ziurys et al. 2007). Along with CS, it may be consuming the majority of the gas-phase sulfur, with little remaining for PS. As a consequence, phosphorus is available to create additional PN. A sensitive astronomical search for PS in VY CMa would certainly help in understanding the complete phosphorus chemical network.

5.4. Phosphorus versus Nitrogen Chemistry

To a first approximation, the chemistry of phosphorus and nitrogen should be fairly similar in circumstellar shells; phosphorus lies directly below nitrogen in the same column of the periodic

table, with similar chemical properties. However, the refractory nature of phosphorus may also affect the comparative gas-phase chemistries between the two atoms.

A comparison of HCP/CP and HCN/CN might be enlightening. The distribution of HCN and CN in IRC +10216 has been mapped in detail by Dayal & Bieging (1995) with the BIMA interferometer. These authors then modeled the observed distributions and determined fractional abundances for both species. The HCN distribution has a peak abundance of $f \sim 3.1 \times 10^{-5}$ and a source radius of $\sim 11''$, while CN has a maximum concentration of $f \sim 3.9 \times 10^{-6}$ and a peak radius of $r \sim 12.5''$. In comparison, the distributions for HCP and CP correspond to radii of $r \sim 11''$ and $r \sim 13''$, respectively, using the same radiative transfer model. Furthermore, the CN/HCN abundance ratio is 0.13 (Dayal & Bieging 1995), while that for CP/HCP is ~ 0.33 . These results suggest that the chemistry of phosphorus is similar to that of nitrogen, at least in IRC +10216.

It should also be noted that the solar P/N ratio is ~ 0.003 and the HCP/HCN ratio in IRC +10216 is ~ 0.001 . The relatively close agreement between the two ratios implies a lack of major nitrogen enrichment in this object. Therefore, PN may represent an avenue by which to estimate the N₂ abundance. Assuming PN/N₂ \sim P/N, the N₂ abundance in IRC +10216 is $\sim 1 \times 10^{-7}$. LTE models have predicted higher values of $f(N_2) \sim 10^{-5}$ to 10^{-4} (MacKay & Charnley 2001; Lafont et al. 1982). The lower value inferred from PN suggests that the majority of the nitrogen in IRC +10216 is locked into HCN.

6. CONCLUSIONS

Phosphorus chemistry appears to be relatively active in both O- and C-rich circumstellar envelopes. Several new species have been found that are not obviously present in molecular clouds, despite the low abundance of phosphorus. While CP is primarily the photodissociation product of HCP in carbon-rich shells, the abundance of PN may principally reflect LTE chemistry in the inner envelope. In the O-rich case, PO appears to be the dominant carrier of phosphorus, although PN is fairly abundant as well. A wider range of sources clearly needs to be investigated for phosphorus-bearing compounds, as well as observations of possible new P-containing species.

We would like to thank the ARO operators and engineering staff. In addition, we would like to acknowledge J. H. Bieging and M. Tafalla for use of their radiative transfer code. This research was supported by NSF grant AST 0607803 and based on work supported by the National Aeronautics and Space Administration through the NASA Astrobiology Institute under Cooperative Agreement CAN-02-OSS-02 issued through the Office of Space Science. D. T. H. is supported by an NSF Astronomy and Astrophysics Postdoctoral Fellowship under award AST-0602282. E. D. T. acknowledges financial support from the NSF Graduate Research Fellowship Program.

REFERENCES

- Agúndez, M., & Cernicharo, J. 2006, ApJ, 650, 374
 Agúndez, M., Cernicharo, J., & Guélin, M. 2007, ApJ, 662, L91
 Ahmad, I. K., & Hamilton, P. A. 1995, J. Mol. Spectrosc., 169, 286
 Arnett, D. 1996, Supernovae and Nucleosynthesis: An Investigation of the History of Matter from the Big Bang to the Present (Princeton: Princeton Univ. Press)
 Beck, C., Schinke, R., & Koput, J. 2000, J. Chem. Phys., 112, 8446
 Bieging, J. H., Shaked, S., & Gensheimer, P. D. 2000, ApJ, 543, 897
 Bieging, J. H., & Tafalla, M. 1993, AJ, 105, 576
 Cernicharo, J., Guélin, M., & Kahane, C. 2000, A&AS, 142, 181
 Clayton, D. 2003, Handbook of Isotopes in the Cosmos (Cambridge: Cambridge Univ. Press)
 Cox, P., Lucas, R., Huggins, P. J., Forveille, T., Bachiller, R., Guilloteau, S., Maillard, J. P., & Omont, A. 2000, A&A, 353, L25
 Cox, P., et al. 1997, A&A, 321, 907
 Dayal, A., & Bieging, J. H. 1995, ApJ, 439, 996
 Fukasaku, S., Hirahara, Y., Masuda, A., Kawaguchi, K., Ishikawa, S., Kaifu, N., & Irvine, W. M. 1994, ApJ, 437, 410
 Grevesse, N., & Sauval, A. J. 1998, Space Sci. Rev., 85, 161
 Guélin, M., Cernicharo, J., Paubert, G., & Turner, B. E. 1990, A&A, 230, L9
 Guélin, M., Muller, S., Cernicharo, J., Apponi, A. J., McCarthy, M. C., Gottlieb, C. A., & Thaddeus, P. 2000, A&A, 363, L9
 Highberger, J. L., Thomson, K. J., Young, P. A., Arnett, D., & Ziurys, L. M. 2003, ApJ, 593, 393
 Humphreys, R. M., Helton, L. A., & Jones, T. J. 2007, AJ, 133, 2716
 Keady, J. J., Hall, D. N. B., & Ridgway, S. T. 1988, ApJ, 326, 832
 Kemper, F., Stark, R., Justtanont, K., de Koter, A., Tielens, A. G. G. M., Waters, L. B. F. M., Cami, J., & Dijkstra, C. 2003, A&A, 407, 609
 Lafont, S., Lucas, R., & Omont, A. 1982, A&A, 106, 201
 Lebouteiller, V., Kuassivi, & Ferlet, R. 2005, A&A, 443, 509
 Lodders, K., & Fegley, B., Jr. 1999, in IAU Symp. 191, Asymptotic Giant Branch Stars, ed. T. Le Bertre, A. Lèbre, & C. Waelkens (San Francisco: ASP), 279
 Maciá, E. 2005, Chem. Soc. Rev. 34, 691
 MacKay, D. D. S., & Charnley, S. B. 2001, MNRAS, 325, 545
 Milam, S. N., Woolf, N. J., & Ziurys, L. M. 2008, ApJ, in press
 Monnier, J. D., Tuthill, P. G., Lopez, B., Cruzalebes, P., Danchi, W. C., & Haniff, C. A. 1999, ApJ, 512, 351
 Müller, H. S. P., Schlöder, F., Stutzki, J., & Winnewisser, G. 2005, J. Mol. Struct., 742, 215
 Nguyen-Q-Rieu, Graham, D., & Bujarrabal, V. 1984, A&A, 138, L5
 Pasek, M. A., & Lauretta, D. S. 2005, Astrobiology, 5, 515
 Pickett, H. M., Poynter, R. L., Cohen, E. A., Delitsky, M. L., Pearson, J. C., & Müller, H. S. P. 1998, J. Quant. Spectrosc. Radiat. Transfer, 60, 883
 Ram, R. S., Tam, S., & Bernath, P. F. 1992, J. Mol. Spectrosc., 152, 89
 Richards, A. M. S., Yates, J. A., & Cohen, R. J. 1998, MNRAS, 299, 319
 Rohlfing, C. M., & Almlöf, J. 1988, Chem. Phys. Lett., 147, 258
 Skinner, C. J., et al. 1997, A&A, 328, 290
 Sopka, R. J., Olofsson, H., Johansson, L. E. B., Nguyen-Q-Rieu, & Zuckerman, B. 1989, A&A, 210, 78
 Tenenbaum, E. D., Woolf, N. J., & Ziurys, L. M. 2007, ApJ, 666, L29
 Tobola, R., Klos, J., Lique, F., Chalasinski, G., & Alexander, M. H. 2007, A&A, 468, 1123
 Truong-Bach, Nguyen-Q-Rieu, Morris, D., & Deguchi, S. 1990, A&A, 230, 431
 Tsuji, T. 1973, A&A, 23, 411
 Turner, B. E., & Bally, J. 1987, ApJ, 321, L75
 Turner, B. E., Tsuji, T., Bally, J., Guélin, M., & Cernicharo, J. 1990, ApJ, 365, 569
 Willacy, K., & Millar, T. J. 1997, A&A, 324, 237
 Young, K., Serabyn, G., Phillips, T. G., Knapp, G. R., Guesten, R., & Schulz, A. 1992, ApJ, 385, 265
 Ziurys, L. M. 1987, ApJ, 321, L81
 Ziurys, L. M., Milam, S. N., Apponi, A. J., & Woolf, N. J. 2007, Nature, 447, 1094